

Constructing a Large Variety of Dirac-Cone Materials in the $\text{Bi}_{1-x}\text{Sb}_x$ Thin Film System

Shuang Tang¹ and M. S. Dresselhaus^{2,3,*}

¹Department of Materials Science and Engineering, Massachusetts Institute of Technology, Cambridge, MA 02139-4037, USA

²Department of Electrical Engineering and Computer Science,

Massachusetts Institute of Technology, Cambridge, MA 02139-4037, USA

³Department of Physics, Massachusetts Institute of Technology, Cambridge, MA 02139-4037, USA

(Dated: October 24, 2018)

We theoretically predict that a large variety of Dirac-cone materials can be constructed in $\text{Bi}_{1-x}\text{Sb}_x$ thin films, and we here show how to construct single-, bi- and tri-Dirac-cone materials with various amounts of wave vector anisotropy. These different types of Dirac cones can be of special interest to electronic devices design, quantum electrodynamics and other fields.

PACS numbers: 73.22.-f, 73.61.At, 73.61.Cw, 73.90.+f, 81.07.-b

Dirac cone materials have recently attracted considerable attention. In an electronic band structure, if the dispersion relation $E(\mathbf{k})$ can be described by a linear function as $E = \mathbf{v} \cdot \mathbf{k}$, where \mathbf{v} is the velocity, \mathbf{k} is the lattice momentum, and $\hbar = 1$, the point where $E \rightarrow 0$ is called a Dirac point. A Dirac cone is a two-dimensional (2D) Dirac point. Dirac cone materials are interesting in electronic device design, quantum electrodynamics and desktop relativistic particle experiments etc. A single-, bi- or tri-Dirac cone system has one, two or three different Dirac cones degenerate in $E(\mathbf{k})$ in the first Brillouin zone. Graphene has two degenerate isotropic Dirac cones at points K and K' in its first Brillouin zone, which is therefore considered as a bi-Dirac-cone system. Many novel phenomena are observed in this system [1], such as the room temperature anomalous integer quantum Hall effect [2], the Klein paradox [3], which means that fermions around a Dirac cone can transmit through a classically forbidden region with a probability of 1. Dirac fermions can be immune to localization effects and can propagate without scattering over large distances on the order of micrometers [4].

In this Letter, we show how to obtain single-, bi- and tri-Dirac-cone $\text{Bi}_{1-x}\text{Sb}_x$ thin films, and how to construct Dirac cones with different anisotropies. We also point out the possibility of constructing semi-Dirac cones in $\text{Bi}_{1-x}\text{Sb}_x$ thin films.

$\text{Bi}_{1-x}\text{Sb}_x$ has many special properties that are interesting from the point of view of anisotropic Dirac cones. We recall that bulk $\text{Bi}_{1-x}\text{Sb}_x$ is a crystalline alloy with a rhombohedral structure, which displays remarkable anisotropy. The first Brillouin zone of bulk $\text{Bi}_{1-x}\text{Sb}_x$ has one T point and three

degenerate L points, $L^{(1)}$, $L^{(2)}$ and $L^{(3)}$, as illustrated in Fig. 1. The bottom of the conduction band is located at the L points, while the top of the valence band can be located either at the T point or at the L points, depending on the Sb composition x when $0 \leq x \leq 0.10$. In bulk $\text{Bi}_{1-x}\text{Sb}_x$, the band structure varies as a function of Sb composition x , temperature T , pressure P and stress τ [5]. The conduction band is very close to the valence band at the L points, so that these bands are non-parabolically dispersed as [6]

$$E(\mathbf{k}) = \pm((\mathbf{v} \cdot \mathbf{k})^2 + E_g^2)^{\frac{1}{2}} \quad (1)$$

due to their strong interband coupling. When the L -point band gap E_g is small, the dispersion relation $E(\mathbf{k})$ becomes linear and Dirac points are formed as $E(\mathbf{k}) \rightarrow \pm \mathbf{v} \cdot \mathbf{k}$. The L -point band gap E_g can approach 0 under some conditions, e.g. when $P = 1$ atm, $E_g \rightarrow 0$ at $x \approx 0.04$ and $T \leq 77$ K [7], or at $x \approx 0.02$ and $T \leq 300$ K [8]. For simplification, this Letter will focus on the low temperature range ($T \leq 77$ K) where the band structure of $\text{Bi}_{1-x}\text{Sb}_x$ does not change much with temperature.

For $\text{Bi}_{1-x}\text{Sb}_x$ thin films, the 2D band structure varies also as a function of film thickness and film growth orientation, which provides considerable flexibility compared to bulk $\text{Bi}_{1-x}\text{Sb}_x$. Furthermore, the quantum confinement effect in the thin film system is potentially interesting, where its anisotropic properties imply potential application possibilities.

The energy spectrum near an L -point Dirac cone in a $\text{Bi}_{1-x}\text{Sb}_x$ thin film is calculated based on the iterative-two-dimensional-two-band model described below. Here the general two band model for two strongly coupled bands obeys the relation [9]

$$\mathbf{p} \cdot \boldsymbol{\alpha} \cdot \mathbf{p} = E(\mathbf{k}) \left(1 + \frac{E(\mathbf{k})}{E_g}\right), \quad (2)$$

where \mathbf{p} is the carrier momentum vector and $\boldsymbol{\alpha}$ is the inverse-mass tensor. The two coupled key parameters $\boldsymbol{\alpha}$ and E_g are calculated in an iterative way in our model as

$$\boldsymbol{\alpha}^{[n]} = \frac{E_g^{[n-1]}}{E_g^{[n]}} \cdot \boldsymbol{\alpha}^{[n-1]} + \frac{1}{m_0} \cdot \left(1 - \frac{E_g^{[n-1]}}{E_g^{[n]}}\right) \cdot \mathbf{I} \quad (3)$$

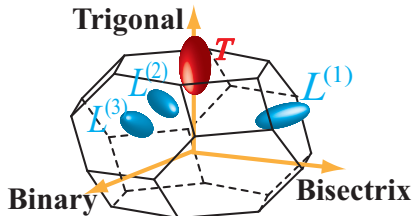


FIG. 1: The 3-fold degenerate L -point electron pockets and the T -point hole pocket in the first Brillouin zone of bulk $\text{Bi}_{1-x}\text{Sb}_x$.

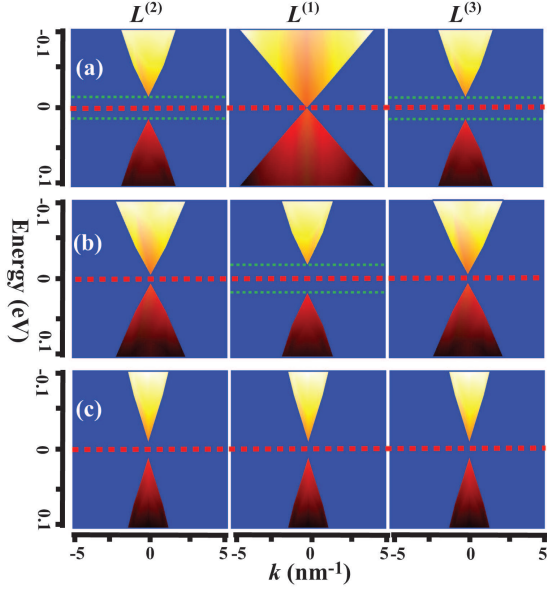


FIG. 2: An illustration of (a) single-, (b) bi- and (c) tri-Dirac-cone $\text{Bi}_{1-x}\text{Sb}_x$ thin films grown along the (a) bisectrix, (b) binary and (c) trigonal axes, respectively. For the cross-sectional view of each cone, \mathbf{k} is chosen such that $\nabla_{\mathbf{k}}E(\mathbf{k})$ has its minimum along that direction of \mathbf{k} . The illustration is based on the example of $\text{Bi}_{1-x}\text{Sb}_x$ thin films with $l_z = 100$ nm, $x = 0.04$, $P = 1$ atm and $T \leq 77$ K, under which the L points of bulk $\text{Bi}_{1-x}\text{Sb}_x$ have a zero-gap. The scenario is similar for other conditions. In (a), a single-Dirac-cone is formed at the $L^{(1)}$ point, while the $L^{(2)}$ - and $L^{(3)}$ - point band gaps are opened up. In (b), two degenerate quasi-Dirac cones are formed at the $L^{(2)}$ and $L^{(3)}$ points, while the $L^{(1)}$ -point band gap is much larger, which leads to a bi-quasi-Dirac-cone material. The band gap at the $L^{(2)}$ and $L^{(3)}$ points can be less than 1 meV if a sample of $l_z = 200$ nm is chosen, which leads to exact Dirac cones. In (c), the $L^{(1)}$ -, $L^{(2)}$ - and $L^{(3)}$ - point band gaps are all the same, and the three quasi-Dirac cones are degenerate in energy.

and

$$E_g^{[n+1]} = E_g^{[n]} + 2 \cdot \frac{\pi^2 \alpha_{33}^{[n]}}{2 \cdot l_z^2}, \quad (4)$$

where m_0 is the free electron mass, \mathbf{I} is the identity matrix, l_z is the film thickness and n denotes the n th step in the iteration. The procedure is repeated until $\alpha^{[n]}$ and $E_g^{[n]}$ become self-consistent, and then we get accurate solutions for $\alpha^{film}(\text{Bi}_{1-x}\text{Sb}_x) = \alpha^{[n]}$ and $E_g^{film}(\text{Bi}_{1-x}\text{Sb}_x) = E_g^{[n]}$ for thin film $\text{Bi}_{1-x}\text{Sb}_x$. Because of the approximations that are valid for Sb composition $0 \leq x \leq 0.10$,

$$\frac{1}{m_0} \cdot \left(1 - \frac{E_g^{[n-1]}}{E_g^{[n]}}\right) \cdot \mathbf{I} \ll \frac{E_g^{[n-1]}}{E_g^{[n]}} \cdot \alpha^{[n-1]}$$

and

$$\left|E_g^{[n+1]} - E_g^{[n]}\right| \ll 2 \cdot \frac{\pi^2 \alpha_{33}^{[n]}}{2 \cdot l_z^2},$$

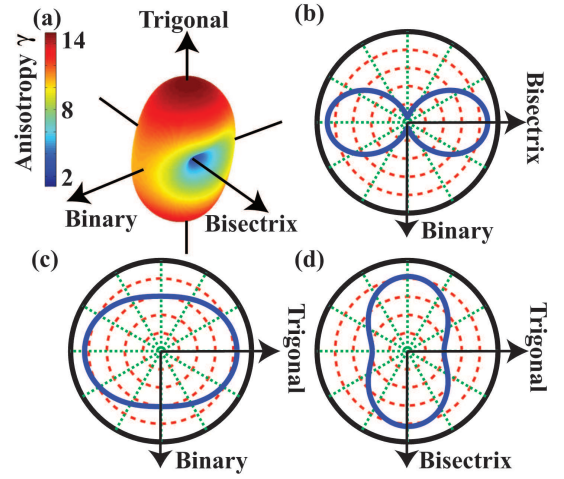


FIG. 3: The anisotropy of the $L^{(1)}$ -point Dirac cone vs. film growth orientation. (a) The anisotropy coefficient γ vs. film growth orientation. The value of γ for a specific film growth orientation is shown by the radius and color. γ can be as large as ~ 14 for films grown along the trigonal axis, and as small as ~ 2 for films grown along the bisectrix axis. \mathbf{v} is shown for the $L^{(1)}$ -point Dirac fermions vs. transport direction for $\text{Bi}_{1-x}\text{Sb}_x$ thin films grown along the (b) trigonal, (c) bisectrix and (d) binary axes. (b)-(c) are drawn based on an example sample with $l_z = 300$ nm and $x = 0.04$.

Eqs. (3) and (4) can be further simplified, which converge to the analytical solution as

$$\alpha^{film}(\text{Bi}_{1-x}\text{Sb}_x) = \frac{\alpha^{bulk}(\text{Bi})}{E_g^{film}(\text{Bi}_{1-x}\text{Sb}_x)} \cdot E_g^{bulk}(\text{Bi}) \quad (5)$$

and

$$E_g^{film}(\text{Bi}_{1-x}\text{Sb}_x) = E_g^{bulk}(\text{Bi}_{1-x}\text{Sb}_x) + \frac{\pi^2 \alpha_{33}^{film}(\text{Bi}_{1-x}\text{Sb}_x)}{l_z^2}. \quad (6)$$

The dispersion relation $E(\mathbf{k})$ can then be solved by the methods used by Ref. [10] from

$$E(\mathbf{k}) + \frac{E^2(\mathbf{k})}{E_g^{film}} = \frac{1}{2} \mathbf{k}^* \cdot \tilde{\alpha} \cdot \mathbf{k} + \frac{\pi^2 \alpha_{33}}{2l_z^2}, \quad (7)$$

where $\tilde{\alpha}_{ij} = \alpha_{i3}\alpha_{j3}/\alpha_{33} - \alpha_{ij}$ for $i, j = 1$ and 2 , and $\alpha = \alpha^{film}(\text{Bi}_{1-x}\text{Sb}_x)$. The Hamiltonian for Bi and $\text{Bi}_{1-x}\text{Sb}_x$ based on $\mathbf{k} \cdot \mathbf{p}$ theory in Eq. (2) is equivalent to a Dirac Hamiltonian with a scaled canonical conjugate momentum [11]. Thus, Eq. (7) is also a good approximation to describe the Dirac cones. The band parameters we use in the present calculations are values that were measured by cyclotron resonance experiments [12].

According to Eqs. (1) and (7), when $E_g \rightarrow 0$ at an L point, the electronic dispersion relation becomes a perfect Dirac cone, where the energy E is exactly proportional to the lattice momentum \mathbf{k} measured from that L point. When E_g becomes large enough [13], the linearity of the dispersion relation becomes an approximation, and the Dirac cone becomes a quasi-Dirac cone. If $\tilde{\alpha}_{11} \gg \tilde{\alpha}_{22}$ with a finite E_g , so that $E \propto k_x$ and

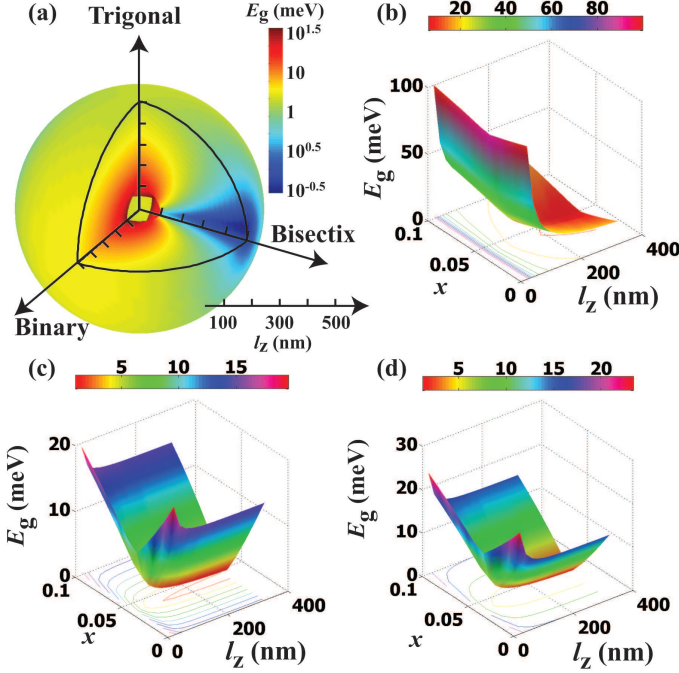


FIG. 4: Scheme for the $L^{(1)}$ -point band gap vs. film growth orientation, film thickness and Sb composition. (a) Illustration of the $L^{(1)}$ -point band gap vs. film growth orientation and film thickness. The radius, direction and color represent the film thickness, film growth orientation and $L^{(1)}$ -point band gap, respectively. The illustration takes $x = 0.04$ as an example. For other Sb compositions ($0 \leq x \leq 0.10$), the film thickness and film growth orientation dependence for the $L^{(1)}$ -point band gap should be similar, which is here illustrated for thin films grown along the (b) trigonal, (c) bisectrix and (d) binary axes.

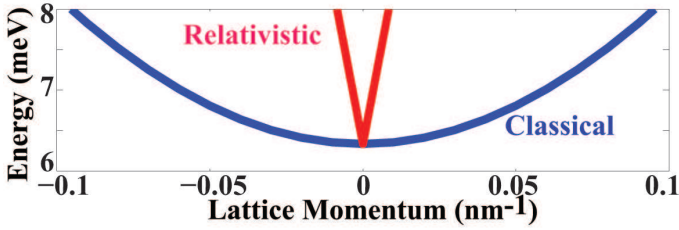


FIG. 5: Example of a semi-Dirac cone in the $\text{Bi}_{1-x}\text{Sb}_x$ thin film system ($x = 0.10$ and $l_z = 100$ nm). It can be seen that around the $L^{(1)}$ point, the fermions are relativistic (linearly dispersed) along the \mathbf{v}_{\max} direction, and classical (parabolically dispersed) along the \mathbf{v}_{\min} direction.

$E \propto k_y^2$, we call it a semi-Dirac cone. In a semi-Dirac cone, the fermions are relativistically dispersed in one direction (k_x), and classically dispersed in another direction (k_y).

We propose that single-, bi- and tri-Dirac-cone materials can be constructed from $\text{Bi}_{1-x}\text{Sb}_x$ thin films, by proper synthesis conditions to control the relative symmetries of the 3 L points. $\text{Bi}_{1-x}\text{Sb}_x$ thin films grown along the bisectrix axis can be single-Dirac-cone materials, as illustrated in Fig. 2a, where the 3-fold degeneracy of the $L^{(1)}$, $L^{(2)}$ and $L^{(3)}$ points is bro-

ken. The value of the film-direction-inverse-mass-component $\alpha_{33}^{film}(\text{Bi}_{1-x}\text{Sb}_x)$ is much smaller for the $L^{(1)}$ point than the corresponding values for the $L^{(2)}$ and $L^{(3)}$ points. The $L^{(1)}$ -point gap $E_g^{(1)}$ is negligibly small due to the small value of $\alpha_{33}^{film}(\text{Bi}_{1-x}\text{Sb}_x)$, where a Dirac cone is formed, as shown in Fig. 2a. However, the $L^{(2)}$ - and $L^{(3)}$ -point band gaps $E_g^{(2)}$ and $E_g^{(3)}$ are much larger, which implies that a single-Dirac-cone at the $L^{(1)}$ point is constructed. Here we are taking advantage of both the extreme anisotropy of $\text{Bi}_{1-x}\text{Sb}_x$ and the quantum confinement effect of thin films. The quantum confinement effects for the $L^{(1)}$ -point carriers differs remarkably from those for the $L^{(2)}$ - and $L^{(3)}$ -point carriers due to the anisotropy of the L -point pockets. Figure 2b shows that a $\text{Bi}_{1-x}\text{Sb}_x$ thin film grown along the binary axis can be a bi-Dirac-cone material, where the $L^{(1)}$ -point band gap $E_g^{(1)}$ is much larger than the $L^{(2)}$ - and $L^{(3)}$ -point band gaps $E_g^{(2)}$ and $E_g^{(3)}$. Thus, $E_g^{(2)}$ and $E_g^{(3)}$ remain small enough [13] to make two degenerate Dirac cones (quasi-Dirac cones) at the $L^{(2)}$ and the $L^{(3)}$ points. In Fig. 2c, the film is grown along the trigonal axis, so that the 3-fold symmetry for the three L points is retained. The three Dirac cones (quasi-Dirac cones) at the $L^{(1)}$, $L^{(2)}$ and $L^{(3)}$ points are degenerate in energy, which makes this film a tri-Dirac-cone material. By definition, an exact Dirac cone has $E_g = 0$. However, $E_g = 0$ Dirac cones are seldom achieved experimentally, so it is practical to consider $E_g \leq k_B T$ as a criterion for an exact Dirac cone. In the temperature range below 77 K that we are considering in this paper, the thermal smearing of $k_B T$ corresponds to ~ 7 meV. For the criterion of a quasi-Dirac cone, we can use $k_B T \leq E_g \leq E_g(\text{Bi})^{bulk}$, where $E_g(\text{Bi})^{bulk} \simeq 14$ meV. Thus, we consider the three Dirac cones in Fig. 2c, as quasi-Dirac cones, which are plotted for the case of $l_z = 100$ nm and $E_g \simeq 10$ meV. If exact Dirac cones are needed, a larger film thickness can be chosen, e.g. $l_z = 200$ nm, which satisfies $E_g \leq k_B T$.

We now show how to construct anisotropic Dirac cones with different shapes for the wave vector as a function of cone angle. To characterize the anisotropy of a Dirac cone, we define an anisotropy coefficient

$$\gamma = \frac{|\mathbf{v}_{\max}|}{|\mathbf{v}_{\min}|}, \quad (8)$$

where \mathbf{v}_{\max} and \mathbf{v}_{\min} are the maximum and minimum in-film carrier group velocities for a Dirac cone that is defined as $\mathbf{v}(\mathbf{k}) = \nabla_{\mathbf{k}} E(\mathbf{k})$. For a perfect Dirac cone, \mathbf{v} is a function of the direction of the lattice momentum \mathbf{k} measured from that L point only and is independent of the magnitude of \mathbf{k} . For an imperfect Dirac cone or a quasi-Dirac cone, this magnitude invariance is exact only when \mathbf{k} is large, and becomes an approximation around the apex when \mathbf{k} is small [13].

Fig. 3 gives us an important guide on how to construct anisotropic $L^{(1)}$ -point Dirac cones. In Fig. 3a, the anisotropy coefficient γ for the $L^{(1)}$ -point Dirac cone as a function of film growth orientation is shown. For a film grown along the bisectrix axis, γ has its minimum value $\gamma_{\min} = \sim 2$, where the

carrier velocity $\mathbf{v}(\mathbf{k})$ for the $L^{(1)}$ -point Dirac cone varies only by a small amount with the direction of \mathbf{k} , as shown in Fig. 3b. For a film grown along the binary axis, $\gamma = \sim 10$, where $\mathbf{v}(\mathbf{k})$ varies more with the direction of \mathbf{k} as shown in Fig. 3c, compared to Fig. 3b. For a film grown along the trigonal axis, γ has its maximum of $\gamma_{max} = \sim 14$, where \mathbf{v} varies significantly with the direction of \mathbf{k} , as shown in Fig. 3d.

Researchers have tried to realize semi-Dirac cones in oxide layers [14], where the fermions are relativistic in one direction and classical in its orthogonal direction. In the present work, we have found that it is possible to construct semi-Dirac cones in the $\text{Bi}_{1-x}\text{Sb}_x$ thin film system. According to Eqs. (1), (2) and (7), for an in-film direction $\hat{\mathbf{k}}$, where $\hat{\mathbf{k}}$ is a unit directional vector of \mathbf{k} in the in-film lattice momentum space, whether the dispersion relation is linear or parabolic depends on the L -point band gap E_g , and the $\tilde{\alpha}$ projection along that direction of $\hat{\mathbf{k}}$, defined by $\tilde{\alpha}_{\hat{\mathbf{k}}} = \hat{\mathbf{k}} \cdot \tilde{\alpha} \cdot \hat{\mathbf{k}}$, where $\tilde{\alpha}$ is given by Eq. (7). When E_g is small and $\tilde{\alpha}_{\hat{\mathbf{k}}}$ is large [13], the energy becomes linearly dispersed along $\hat{\mathbf{k}}$; when E_g is large and $\tilde{\alpha}_{\hat{\mathbf{k}}}$ is small, the energy becomes parabolically dispersed along $\hat{\mathbf{k}}$. To construct a semi-Dirac cone, we need to find a proper L -point band gap E_g and anisotropy γ , such that $E_g/\tilde{\alpha}_{max}$ is small and E_g/α_{min} is large. In this case, the electronic energy is linearly dispersed along the $\tilde{\alpha}_{max}$ direction and parabolically dispersed along the α_{min} direction. Here $\tilde{\alpha}_{max}$ and $\tilde{\alpha}_{min}$ are the maximum and minimum values of $\tilde{\alpha}_{\hat{\mathbf{k}}}$, which correspond to the principal axes of the 2D tensor $\tilde{\alpha}$. The L -point band gap varies as a function of the film thickness l_z , the growth orientation and the Sb composition x , as shown by the calculated results given in Fig. 4. To construct a semi-Dirac cone, we need to find a growth direction that ensures a significant anisotropy, and a large enough value of E_g which ensures that $E(\mathbf{k})$ becomes parabolically dispersed along the $\tilde{\alpha}_{min}$ direction. However, the E_g should not be too large, because of the necessity that the linear dispersion relation along the $\tilde{\alpha}_{max}$ direction is maintained. These requirements can all be achieved by choosing the proper Sb composition x , film thickness l_z and growth orientation as shown in Fig. 4. From Figs. 2 and 3, we know that the $L^{(1)}$ -point Dirac cone has a maximum \mathbf{k} -vector anisotropy, when the growth orientation is near the trigonal axis. We also see that the thin film becomes a single-Dirac-cone material when the growth direction is near the bisectrix axis. Thus, a good strategy to construct a semi-Dirac cone is to choose a growth orientation between the trigonal and the bisectrix axis, in the trigonal-bisectrix plane. An example of a semi-Dirac cone is shown in Fig. 5, where the example sample is grown along a direction that is 40° from the trigonal

axis, 50° from the bisectrix axis, and perpendicular to the binary axis. Thus, a large Sb composition (e.g. $x \approx 0.10$) and a small film thickness (e.g. $l_z \approx 100$ nm) is preferred to make the E_g large, and $x = 0.10$ and $l_z = 100$ nm are chosen for this example sample.

In conclusion, we have proposed the growth of $\text{Bi}_{1-x}\text{Sb}_x$ thin films, which for selected concentrations of Sb and different directions to the film normal allows different Dirac-cone materials to be constructed. We have shown how to construct single-, bi- and tri-Dirac-cone materials, as shown in Fig. 2, as well as quasi- and semi-Dirac-cone materials, as shown in Fig. 2c and Fig. 5, respectively.

The authors acknowledge the support from AFOSR MURI Grant number FA9550-10-1-0533, sub-award 60028687. The views expressed are not endorsed by the sponsor.

* millie@mgm.mit.edu

- [1] A. Neto *et al.*, *Rev. Modern Phys.* **81**, 109 (2009)
- [2] K. Novoselov *et al.*, arXiv: cond-mat/0509330; Y. Zhang *et al.*, *Nature (London)* **438**, 201 (2005).
- [3] A. Calogeracos and N. Dombey, *Cont. Phys.* **40**, 313 (1999); C. Itzykson and J. Zuber, *Quantum Field Theory* (Dover, New York, 2006).
- [4] K. Novoselov *et al.*, *Science* **306**, 666 (2004).
- [5] A. Jain, *Phys. Rev.* **114**, 1518 (1959); S. Tanuma, *J. Phys. Soc. Jpn* **16**, 2349 (1961); S. Golin, *Phys. Rev.* **176**, 830 (1968); K. Hiruma *et al.*, *Sol. State Commun.* **38**, 859 (1981).
- [6] D. Hsieh *et al.*, *Nature (London)* **452**, 970 (2008).
- [7] M. Vecchi, J. Pereira, and M. Dresselhaus, *Phys. Rev. B* **14**, 298 (1976); P. Chao, H. Chu and Y. Kao, *Phys. Rev. B*, **9**, 4030 (1974).
- [8] E. Rogacheva, *J. Phys. Chem. Sol.* **69**, 580 (2008).
- [9] B. Lax and J. Mavroides, *Solid State Physics* (Acad. Press, New York, 1960), Vol. 11.
- [10] Y. Lin, X. Sun and M. Dresselhaus, *Phys. Rev. B* **62**, 4610 (2000). O. Rabin, Y. Lin and M. Dresselhaus, *Appl. Phys. Lett.* **79**, 81 (2001).
- [11] F. Buot, *Phys. Rev. A* **8**, 1570 (1973).
- [12] R. Dinger and A. Lawson, *Phys. Rev. B* **7**, 5215 (1973); R. Isaacson and G. Williams, *Phys. Rev.* **185**, 682 (1969); W. Datars and J. Vanderkooy, *IBM J. Research and Development* **8**, 247 (1964).
- [13] Based on Eq. (1), when E_g is large enough of \mathbf{k} is small enough so that $E_g \ll |\mathbf{v} \cdot \mathbf{k}|$, $E(\mathbf{k})$ can be considered as linearly dispersed along \mathbf{k} .
- [14] S. Banerjee *et al.*, *Phys. Rev. Lett.* **103**, 01640 (2009); V. Pardo, V. and W. Pickett, *Phys. Rev. Lett.* **102**, 166803 (2009).